OPEN

NPG Asia Materials (2016) 8, e330; doi:10.1038/am.2016.178
www.nature.com/am

ORIGINAL ARTICLE

Centimeter-sized epitaxial h-BN films

Hongseok Oh[1], Janghyun Jo[2], Youngbin Tchoe[1], Hosang Yoon[1], Hyun Hwi Lee[3], Sung-Soo Kim[4], Miyoung Kim[2], Byeong-Hyeok Sohn[4] and Gyu-Chul Yi[1]

We report the growth and transfer of centimeter-sized, epitaxial hexagonal boron nitride (h-BN) few-layer films using Ni(111) single-crystal substrates. The h-BN films were heteroepitaxially grown on 10×10 mm^2 or 20×20 mm^2 Ni(111) substrates using atmospheric pressure chemical vapor deposition with a single ammonia-borane precursor. The grown films were transferred to arbitrary substrates via an electrochemical delamination technique, and the remaining Ni(111) substrates were repeatedly re-used. A careful analysis of the growth parameters revealed that the crystallinity and area coverage of the h-BN films were mostly sensitive to the sublimation temperature of the ammonia-borane source. Moreover, various physical characterizations confirmed that the grown films exhibited the typical characteristics of hexagonal boron nitride layers over the entire area. Furthermore, the heteroepitaxial relationship between h-BN and Ni(111) and the overall crystallinity of the film were thoroughly investigated using a synchrotron radiation X-ray diffraction analysis including θ–2θ scans, grazing incident diffraction, and reciprocal space mapping. The crystallinity at the microscopic scale was further investigated using transmission electron microscopy (TEM)-based techniques, including selective area electron diffraction pattern mapping, electron back-scattered diffraction, and high-resolution TEM.

NPG Asia Materials (2016) **8,** e330; doi:10.1038/am.2016.178; published online 25 November 2016

INTRODUCTION

Hexagonal boron nitride (h-BN) is a dielectric insulator with a two-dimensional layered structure. It is an appealing substrate dielectric for many applications owing to its favorable properties, such as a wide band gap energy of 5.6–6.0 eV, chemical inertness of the surface and high thermal conductivity.[1–4] Furthermore, its remarkable mechanical strength makes it possible to use few-layered h-BN as a flexible and transparent substrate, which is ideal for next-generation electronics and optoelectronics in applications such as flexible and transparent transistors or light-emitting devices.[5–9] However, the difficulty of preparing high-quality large-area h-BN films has hindered their widespread use. While exceptionally clean and ordered h-BN layers can be prepared from bulk crystals by mechanical cleavage methods,[10,11] their limited sizes and random thicknesses and orientations are not suitable for practical device applications. However, the large-area h-BN layers prepared by chemical vapor deposition usually exhibit polycrystalline structures with a typical average grain size of several microns[12–14] or tens of microns.[15,16] Grain boundaries or dislocations in polycrystalline h-BN can affect its electronic or mechanical properties, resulting in a lower band gap energy, higher leakage current and poorer mechanical strength.[17–20] Accordingly, large-area single crystalline h-BN layers are desired to fully realize the potential advantages of h-BN in device applications. To this end, efforts on controlling the size and direction of individual domains of h-BN have been reported;[15,16,21,22] however, obtaining large-scale single crystalline h-BN films remains challenging. Here, we report the synthesis of epitaxial h-BN films on the centimeter scale while maintaining a low cost of production by re-using the Ni(111) substrates via electrochemical delamination.

The use of Ni(111) for heteroepitaxial growth of h-BN has been previously reported,[23–26] in particular for obtaining monolayer h-BN on Ni(111).[25,27] In those studies, substrates were heated in an ultra-high vacuum chamber, and exposure to the borazine vapor resulted in the formation of a h-BN layer. Similarly, Ni(110), Ru(0001) and Rh (111) substrates were also used as the substrates to heteroepitaxially grow h-BN layers.[28,29] However, it was difficult to separate such epitaxial h-BN films from the original substrates without consuming them; therefore, their further characterization and potential applications were limited. In this work, h-BN layers were separated using an electrochemical delamination technique, and the Ni(111) substrates were reusable. Furthermore, we investigated microstructural characteristics of the free-standing h-BN films.

MATERIALS AND METHODS

Growth of h-BN film

Polished 10×10 mm^2 or 20×20 mm^2 Ni(111) single crystals were purchased from commercial vendors (Crystal Bank at Pusan National University, Korea or MTI Korea, Seoul, Korea). The substrates were further chemically–mechanically polished by a commercial polishing service to obtain a smooth

[1]Department of Physics and Astronomy, Institute of Applied Physics, and Research Institute of Advanced Materials (RIAM), Seoul National University, Seoul, Korea; [2]Department of Materials Science and Engineering, and Research Institute of Advanced Materials (RIAM), Seoul National University, Seoul, Korea; [3]Pohang Accelerator Laboratory, Pohang University of Science and Technology (POSTECH), Pohang, Korea and [4]Department of Chemistry, Seoul National University, Seoul, Korea
Correspondence: Professor G-C Yi, Department of Physics and Astronomy, Institute of Applied Physics, and Research Institute of Advanced Materials (RIAM), Seoul National University, 1 Gwanak-ro, Gwanak-gu, Seoul 08826, Korea.
E-mail: gcyi@snu.ac.kr
Received 26 April 2016; revised 26 September 2016; accepted 27 September 2016

surface. The root-mean-square surface roughness value obtained over a scanned area of $5 \times 5\ \mu m^2$ was 3 nm. The smooth surface of the substrates is important for the preparation of high-quality h-BN films because rough surfaces of the as-received Ni crystals contained grains with unwanted crystal orientations. An ammonia-borane solid precursor and the Ni(111) crystal were loaded in each heating zone of a two-zone furnace in an atmospheric pressure chemical vapor deposition system (Supplementary Figure S1a). The temperatures of each zone were carefully selected to precisely control the sublimation rate of ammonia-borane and the growth of h-BN films (Supplementary Figure S1b). A mixture of high-purity argon and hydrogen (800/200 sccm of Ar/H_2 flow) was flown in the reactor to purge the gas inside the reactor. The Ni(111) single crystal was heated to 800–1030 °C for 1 h, after which ammonia-borane was heated to 90–100 °C for slow sublimation. The Ar/H_2 gas flow was maintained at 800/200 sccm during the growth. After 1 h of growth, the furnace was cooled down naturally to room temperature.

Electrochemical delamination

The h-BN films grown on the Ni(111) substrates were transferred by an electrochemical delamination method. For the film transfer, poly(methyl methacrylate) (PMMA) was spin-coated on the h-BN/Ni(111) stack at 4000 r.p.m. for 1 min, and baked at 180 °C for 1 min. Then, a Ni foil and the PMMA/h-BN/Ni(111) stack were connected to the anode and cathode of a DC power supply, respectively. Both electrodes were dipped into a 0.1 M NaOH solution. Then, a bias voltage of 10 V with a current of 0.3–1.0A was applied during this process. The PMMA/h-BN films were slowly separated from the Ni(111) surface by hydrogen bubbles. After the PMMA/h-BN was completely detached, the floating films were transferred to deionized water for rinsing, and then finally transferred onto SiO_2/Si or quartz substrates for further characterization. After the films were dried at room temperature, the PMMA layers were dissolved in acetone. In contrast, the Ni(111) substrates were cleaned by sonication in acetone and isopropanol after the delamination and used to grow more h-BN films. The crystal structure of the Ni(111) has been investigated using electron back-scattered diffraction accompanied by scanning electron microscope (SEM-EBSD). SEM-EBSD analysis was performed using SU70 (Hitachi High-Technologies Corporation, Tokyo, Japan) equipped with field-emission gun.

Synchrotron radiation X-ray diffraction

Synchrotron radiation X-ray diffraction (SR-XRD) analyses, including theta–2theta (θ–2θ) scans, grazing incidental diffraction (GID), reciprocal lattice mapping and azimuthal angle (ϕ) scans were carried out at the 5A beamline of Pohang Acceleration Laboratory in Korea. The X-ray wavelengths used for SR-XRD were 0.693Å for θ–2θ and ϕ scans, and 1.071Å for GID measurements and reciprocal space mapping analysis. The measurements at different X-ray wavelengths were carried out at different dates.

Transmission electron microscopy

Transmission electron microscopy (TEM) was used for the structural characterization; specifically, a FEI Tecnai G2 F20 (FEI Company, Hillsboro, OR, USA) was used for selective area electron diffraction (SAED) pattern mapping, a JEM-2100F (JEOL Ltd, Tokyo, Japan) equipped with ASTAR (NanoMEGAS SPRL, Brussels, Belgium) was used for EBSD analysis and a Titan 80-300 (FEI Company) was used for high-resolution imaging and analysis. Cross-sectional TEM samples were prepared by the focused ion beam technique.

Atomic force microscopy

Surface morphologies of h-BN films and Ni substrates were investigated using an atomic force microscope (AFM). For the AFM imaging, a high-aspect-ratio cantilever (AR5, NanoWorld AG, Neuchatel, Switzerland) with a resonant

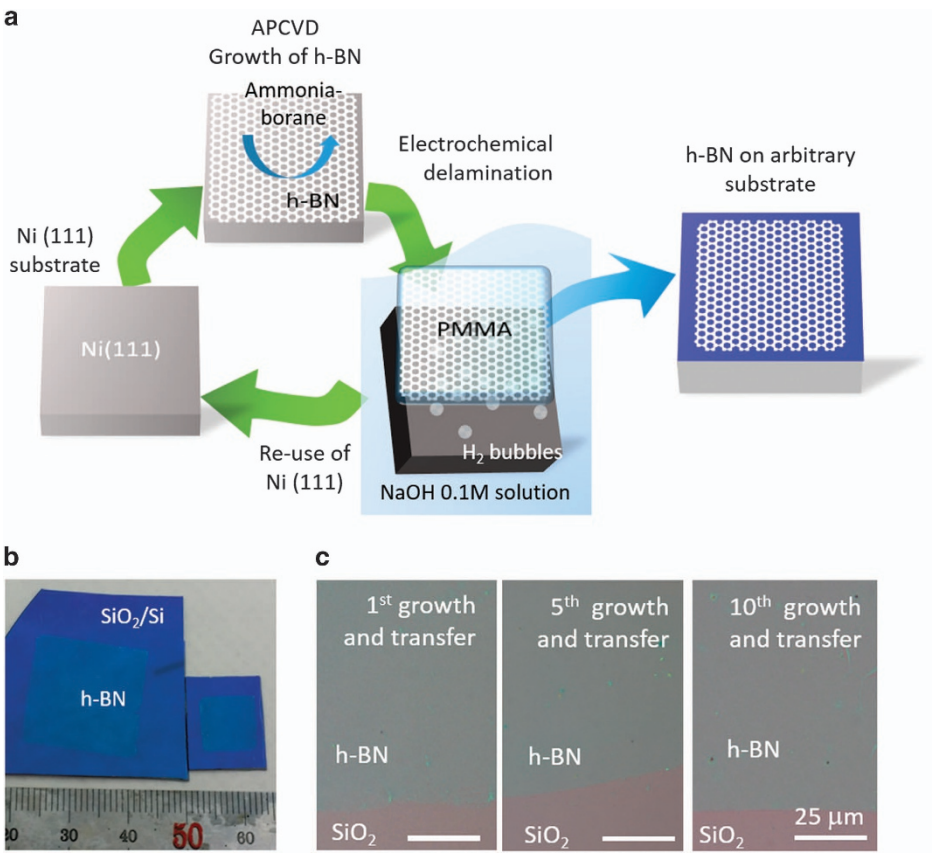

Figure 1 Repeated growth and transfer of h-BN films using Ni(111) single-crystal substrate. (**a**) Schematic illustration of the experiment. (**b**) h-BN films transferred onto SiO_2/Si substrates. (**c**) Optical microscope images of h-BN films on SiO_2/Si substrates obtained from the same Ni(111) substrate with different numbers of uses. APCVD, atmospheric pressure chemical vapor deposition; h-BN, hexagonal boron nitride.

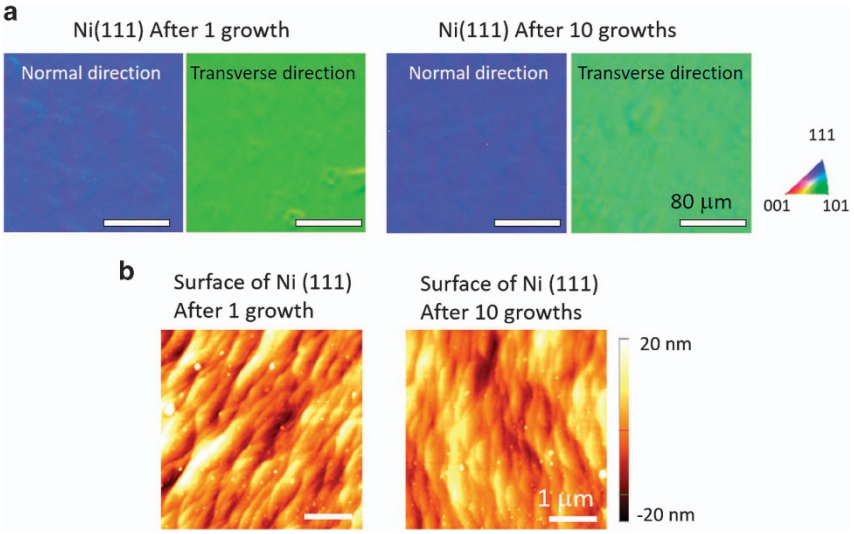

Figure 2 (**a**) EBSD IPF maps of the Ni(111) substrate in the normal direction (ND) and the transverse direction (TD) after one and 10 growths. (**b**) AFM image of Ni(111) substrate after one and 10 growths. AFM, atomic force microscope; EBSD, electron back-scattered diffraction; IPF, inverse pole figure.

frequency of 330 kHz was used. The AFM experiments were performed on the surface area of 5 μm × 5 μm under tapping mode. The AFM was also used to estimate the thickness of the h-BN films.

Other characterizations

Physical characteristics of h-BN films were further investigated using Raman spectrum mapping, optical microscopy, AFM, ultraviolet–visible–infrared spectroscopy transmittance measurements, and X-ray photoelectron spectroscopy. The Raman spectra were measured using a spectrometer (Horiba Jobin-Yvon LabRam Aramis spectrometer, Horiba Ltd, Kyoto, Japan) with a focal length of 460 mm and a wavelength of 514.5 nm with an Ar-ion laser as the excitation source. Raman mapping was performed in a 10 μm × 10 μm region with a step size of 0.2 μm. The absorption spectra were investigated using ultraviolet–visible–infrared spectroscopy (Cary 5000 ultraviolet–visible–near-infrared, Agilent Technologies, Santa Clara, CA, USA). The h-BN films transferred onto quartz substrates were used to investigate the absorbance curve. To extract the optical band gap of h-BN layers, the absorbance curve of the h-BN film was converted to a Tauc's plot (Supplementary Figure S3d, inset) using Tauc's equation.[30] The chemical compositions of the films were determined by X-ray photoelectron spectroscopy (AXIS-HSi, Kratos Analytical Ltd, Manchester, UK). Before the X-ray photoelectron spectroscopy measurements, h-BN films were transferred onto SiO_2/Si substrates. The X-ray photoelectron spectroscopy measurements were carried out under ultra-high vacuum condition (5×10^{-9} torr) using Mg-Kα X-ray as the excitation source.

RESULTS AND DISCUSSION

Heteroepitaxial growth and transfer of h-BN film on Ni(111)

The h-BN films were grown on Ni(111) single-crystal substrates by atmospheric pressure chemical vapor deposition and transferred onto arbitrary substrates, as schematically illustrated in Figure 1a. Before the growth of h-BN films, the surface of the Ni(111) substrates was polished by chemical–mechanical planarization, after which Ni(111) could be repeatedly re-used. Then, a two-zone furnace system with a single ammonia-borane solid precursor was used to grow h-BN films on the Ni substrates. The as-grown h-BN films were spin-coated with PMMA and then transferred onto foreign substrates using the electrochemical delamination method.[14,31] The transferred h-BN films can easily be identified by the naked eye, as shown in Figure 1b. The size of the h-BN films is limited by that of the Ni(111) substrate; in this work, we report h-BN films as large as $20 \times 20\ mm^2$ (the maximum size of commercially available Ni(111)). After the transfer process, Ni(111) substrates were cleaned and re-used repeatedly to grow additional h-BN films. The detailed procedures are described in the 'Materials and methods' section.

The morphology of the repeatedly obtained h-BN films and the reliability of the growth and transfer processes were first investigated using optical microscopy. The optical microscope images of h-BN films transferred onto SiO_2/Si substrates are shown in Figure 1c. Over the entire image, h-BN films exhibit a uniform difference in the color contrast with the SiO_2/Si surface, which indicates that the thickness of the h-BN films is uniform at the nanometer scale over the entire region.[32] This uniform growth of h-BN films on Ni(111) single-crystal substrates is in strong contrast to that on poly-crystalline Ni foils, whose resulting films grown under the same growth conditions show multiple h-BN patches with varying thicknesses (Supplementary Figure S1c). Considering the dissimilar growth rate of h-BN on different crystal plane orientations of the nickel substrate, the uniform thickness of h-BN films on Ni(111) presumably results from the single crystallinity of the substrate.[33,34] In addition, as shown in Figure 1c, the same optical contrast was observed from the first, fifth and tenth grown and transferred h-BN films, which indicates that h-BN films with a uniform thickness were repeatedly obtained.

The crystal structure and surface morphology of Ni(111) were examined by SEM-EBSD and AFM between the repeated growth and transfer processes to confirm that the Ni(111) substrates can be reliably re-used. Figure 2a shows the inverse pole figure (IPF) color map SEM-EBSD images for a Ni(111) substrate after the first and tenth growth and transfer processes. In the IPF color map after the first growth and transfer process, the whole surface exhibited the same blue color in the normal direction and the same green color in the transverse direction (TD), which indicates that the whole region is oriented in the (111) direction. The IPF color map after the tenth growth and transfer process was almost identical, which indicates that the crystal structure of the Ni(111) substrate remained the same in this region after multiple growth and transfer processes, without forming additional disoriented grains at elevated temperatures during h-BN growth. In addition, as shown in Figure 2b, even after 10 cycles of repeated growth and transfer processes, there were no significant changes in the film surface morphology as follows: the atomic terraces remained largely identical, and no significant increase in surface

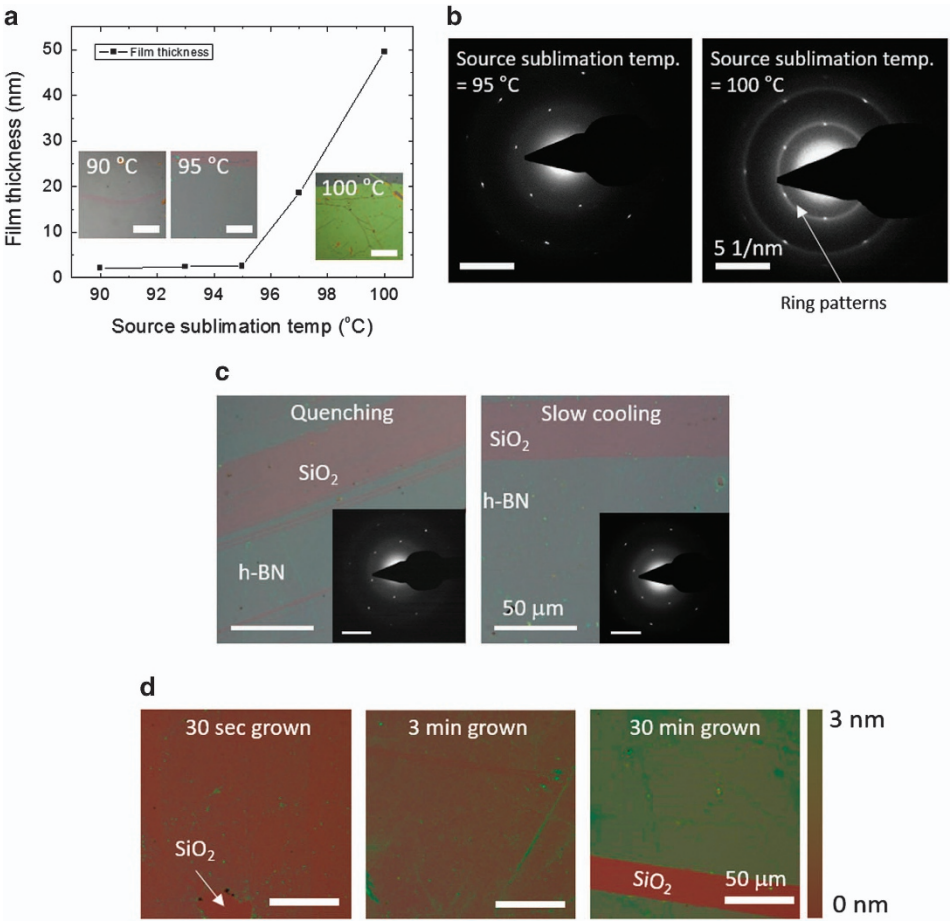

Figure 3 Growth behavior of h-BN film on Ni(111) using APCVD. (**a**) Thickness of h-BN films grown at different ammonia-borane sublimation temperatures. Insets are optical microscope images of the film on SiO_2/Si substrates. Scale bar, 50 μm. (**b**) SAED pattern of h-BN films with ammonia-borane sublimation temperatures of 95 °C and 100 °C. (**c**) Optical microscope images of h-BN films with different cooling rates. Insets are corresponding SAED patterns of the h-BN films. Scale bar, 5 nm^{-1} (**d**) High saturation optical microscope images of h-BN films transferred onto SiO_2/Si substrates with different growth times. APCVD, atmospheric pressure chemical vapor deposition; h-BN, hexagonal boron nitride; SAED, selective area electron diffraction.

roughness was observed. Both the EBSD and AFM studies on the Ni(111) substrate strongly suggest that the crystal structure and surface morphology of Ni(111) substrates were not affected by the repeated growth and transfer processes.

Effect of growth parameters

We investigated the effects of growth parameters, including the sublimation temperature of the ammonia-borane precursor and the film growth temperature, on the characteristics of h-BN films (Supplementary Figure S1b). Figures 3a and b shows the resulting changes in thickness, coverage and crystallinity of the h-BN films grown at the various ammonia-borane sublimation temperatures of 90–100 °C. The temperature of zone #2 was maintained at 875 °C. The films grown with sublimation temperatures of 90 and 93 °C exhibited incomplete coverage (left in Supplementary Figure S2a) over a large area and a very small increase in the thickness from 2.5 to 3 nm. However, the films with a sublimation temperature of 95 °C showed sufficient area coverage (Figure 3a, inset) and a clear dot pattern in the SAED image (left in Figure 3b), and, hence, we used this temperature for all other analyses in this work. However, when the sublimation temperature was increased to 97 and 100 °C, the thickness increased dramatically to 20 and 50 nm, respectively. However, these thick films exhibited distinct ring patterns in their SAED images as a result of the presence of randomly oriented crystal structures (right in Figure 3b), and thus these films were less crystalline than the 95 °C sample. On the basis of these results, it is very important to carefully control the sublimation temperature of ammonia-borane to obtain a fully covered, few-layered film of high crystallinity. It should be noted that by increasing the growth time from 30 min to 3 hours, complete coverage was achieved even at a low sublimation temperature of 93 °C, as shown in the image in the right of Supplementary Figure S2a. Likewise, the growth temperature in zone #2 had a role in controlling the growth, albeit a less critical role. The temperature of zone #1 was maintained at 95 °C. An adequate growth temperature range in our system was determined as 875–950 °C, while a low temperature of 800 °C resulted in slow growth and low coverage, and a high temperature of 1030 °C resulted in faster growth but unsatisfactory crystallinity (Supplementary Figure S2b). It is noteworthy that polycrystalline structure of the h-BN film grown at 1030 °C can also result from unwanted heating due to radiation from zone #2 because the crystallinity and thickness are very sensitive to the ammonia-borane sublimation temperature.

The effect of varying the cooling rate was also investigated to clarify the governing growth mechanism. The cooling rate of the substrate was varied by opening the top cover of the chamber after the growth was completed; this increased the initial cooling rate from

10 °C min^{-1} to >50 °C min^{-1}. The temperatures of zones #1 and #2 were 95 °C and 900 °C, respectively. Generally, a precipitation-driven growth is expected to be strongly affected by the change in cooling rate, while a surface-mediated growth would be minimally affected.[35,36] In our case, Figure 3c shows that the film thickness, uniformity, and crystallinity were nearly identical for both fast and slow cooling, which indicates that a surface-mediated growth was more likely. This is presumably attributed to the low dissolution rate of other reactants into the Ni(111) facet owing to its low surface energy.[33]

The initial growth mode was investigated by reducing the growth duration. In this case, h-BN films with growth durations of 30 s, 3 min and 30 min were transferred to SiO_2/Si substrates and compared using optical microscopy (Figure 3d). The growth of h-BN in our experiments appears to be initiated from dense, multiple points on the Ni(111) surface, which already cover a large percentage of the whole area of the surface even after a duration of 30 s. This is in contrast to previous chemical vapor deposition works where individual grains with a low density grew larger and then covered the entire film.[15,16,21] As the growth time increases, each h-BN nucleus merged into several multilayered h-BN patches, and then films with complete coverage were finally formed (see Supplementary Figures S3a,b and Supplementary Information). Nevertheless, in our case, a strong epitaxial relationship between the h-BN film and the Ni(111) surface presumably led to the formation of a single-oriented h-BN film.

Heteroepitaxial relationship and crystallinity

The heteroepitaxial relationship and overall crystallinity of h-BN films on Ni(111) were investigated using SR-XRD. Figure 4a shows a θ–2θ scan of the as-grown h-BN on Ni(111), with only peaks from h-BN(0002) and Ni(111) planes observed. This indicates that the *c* axis of the h-BN film is normal to the Ni surface plane. More importantly, we used GID to verify the crystallinity along the in-plane direction. With a beam at an incident angle of 0.3° in our experiments, the area of the illuminated surface was 0.4×10 mm^2, which enabled a centimeter-scale investigation of the in-plane crystallinity. Figure 4b shows high-resolution GID spectra of h-BN/Ni(111) obtained at two different sample orientations separated from each other by 30°. A strong and sharp h-BN(10$\bar{1}$0) peak was observed along the Ni<$\bar{1}\bar{1}$2> direction, with no other h-BN related peaks, which indicates the presence of a well-ordered h-BN crystal with a single orientation throughout the whole surface interaction area. However, measurement along the Ni<10$\bar{1}$> direction (that is, a 30° rotation from Ni<$\bar{1}\bar{1}$2>) exhibited peaks from h-BN(11$\bar{2}$0) and Ni(20$\bar{2}$), which are not clearly separated due to their similar *d*-spacing values (1.252 Å for h-BN(11$\bar{2}$0) and 1.246Å for Ni(20$\bar{2}$)).[37]

The in-plane crystallinity of the h-BN films was further investigated by XRD scans of the h-BN{10$\bar{1}$0} peak as a function of the substrate angle (or azimuthal angle) ϕ. Owing to the elongated surface footprint of up to 10 mm, this ϕ-scan probes the distribution of in-plane crystal orientation over a wide centimeter-scale area. As shown in Figure 4c, the resulting plot from as-grown h-BN on Ni exhibits diffraction peaks from h-BN{10$\bar{1}$0} only at ϕ values of exact multiples of 60°, thus confirming a clear six-fold symmetry of h-BN. A small angular dispersion with a full width at half maximum value of 0.8° was observed. Furthermore, the θ–2θ scan, GID, and ϕ-scan results were nearly identical after the h-BN film was delaminated and transferred onto a SiO_2/Si substrate (Supplementary Figure S4).

We investigated the epitaxial relationship between the h-BN film and Ni substrate using SR-XRD reciprocal space mapping. Figure 4d shows a HK-mesh contour plot of the reciprocal space mapping, which shows an exact overlap of two peaks from h-BN(11$\bar{2}$0) and Ni(20$\bar{2}$). The diffraction peak from Ni(20$\bar{2}$) was sharp in the Q_y-direction, with its value matching well with known values (*d*-spacing of 1.246 Å or Q_y-value of 5.041 Å^{-1}), but spread out in the Q_x-direction, as commonly observed for other single crystal

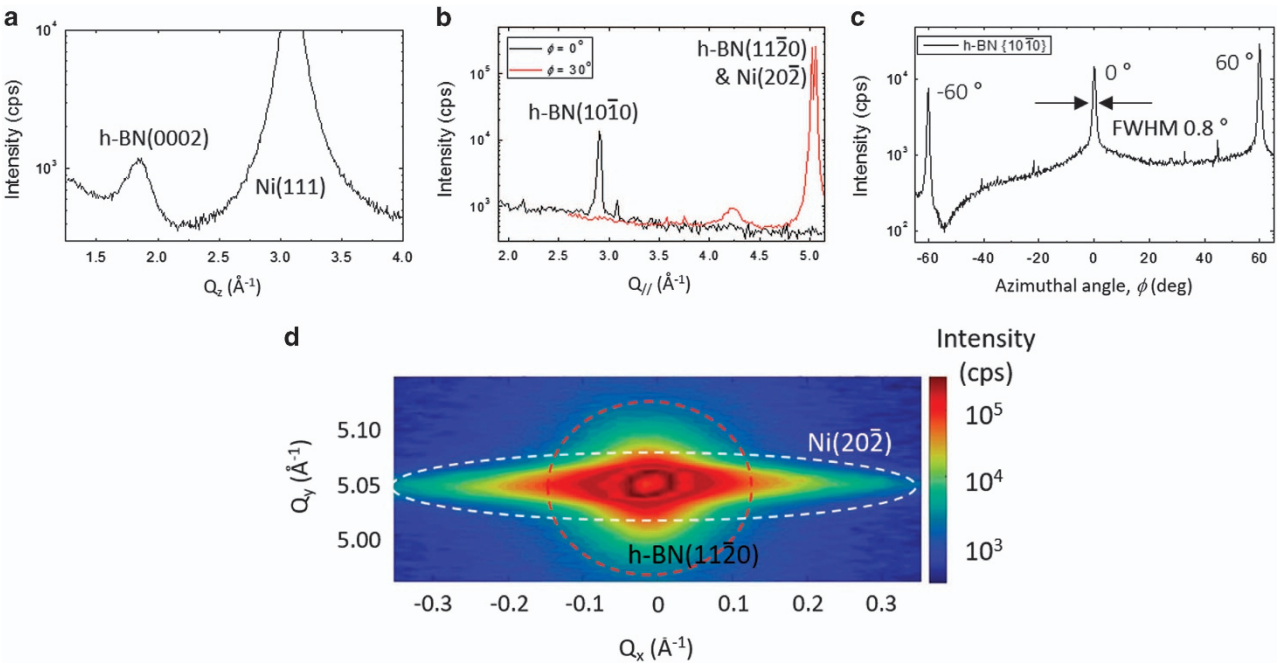

Figure 4 Synchrotron radiation X-ray diffraction (SR-XRD) profiles of h-BN film grown on Ni(111) substrate. (**a**) θ–2θ scan of as-grown h-BN/Ni(111). (**b**) Grazing incident diffraction (GID) profile of h-BN/Ni(111) with different X-ray azimuthal angles, separated by 30°. (**c**) Azimuthal angle(ϕ)-scan of h-BN{10$\bar{1}$0} plane from as-grown h-BN/Ni, showing six-fold symmetry. (**d**) HK-mesh contour maps of reciprocal space mapping (RSM) around h-BN(11$\bar{2}$0) and Ni(20$\bar{2}$) diffraction peaks. h-BN, hexagonal boron nitride.

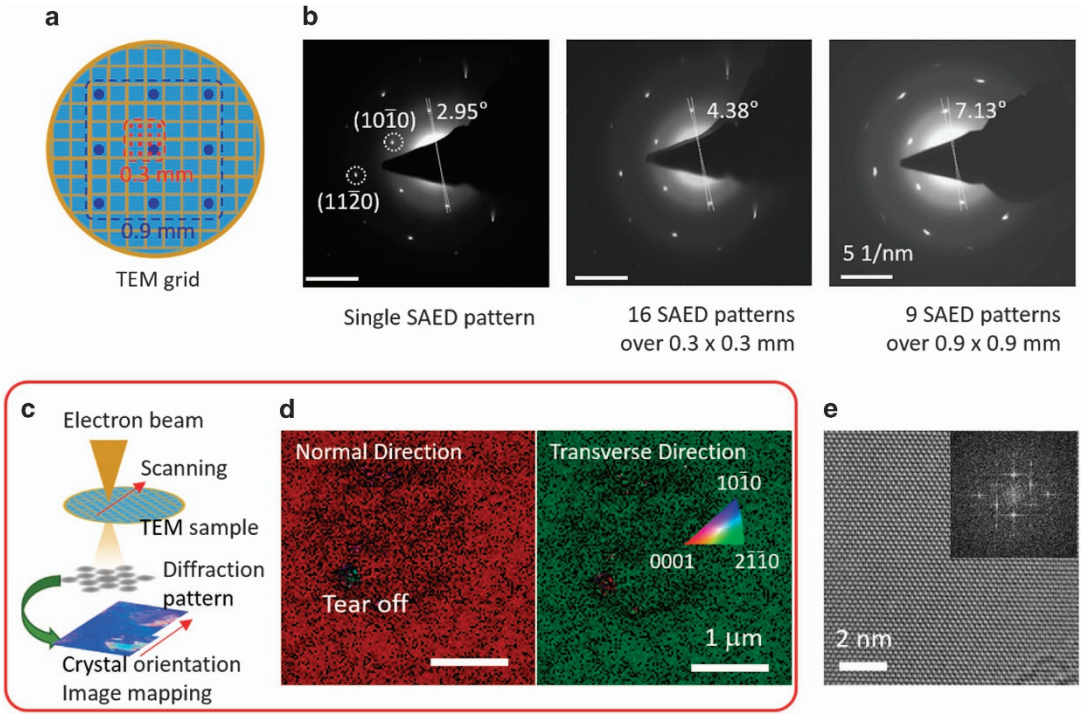

Figure 5 Microstructural analysis of h-BN film using TEM. (**a**) Schematic image of the SAED mapping analysis. (**b**) SAED image of a h-BN film from a single spot, and overlaid SAED mapping images from 16 SAED patterns over a 0.3×0.3 mm^2 area and 9 SAED patterns over a 0.9×0.9 mm^2 area. (**c**) Schematic illustration of the TEM-EBSD analysis, which is used to visualize the real-space crystal structure. (**d**) TEM-EBSD IPF maps of h-BN film in normal direction (ND) and transverse direction (TD). (**e**) HR-TEM image of h-BN film. FFT image is shown in the inset. EBSD, electron back-scattered diffraction; FFT, fast-Fourier-transformed; h-BN, hexagonal boron nitride; HR, high resolution; IPF, inverse pole figure; SAED, selective area electron diffraction; TEM, transmission electron microscopy.

metallic substrates.[38] However, the diffraction peak from h-BN(11$\bar{2}$0) was situated at a larger Q_y-value than expected (d-spacing of 1.252 Å or Q_y-value of 5.019 Å^{-1}). Furthermore, while its spread in the Q_x-direction (estimated as a width at 10% maximum of 0.13 Å^{-1}, which corresponds to a 1.5° spread in ϕ-scan) was in accordance with the full width at half maximum observed in Figure 4c, its spread in the Q_y-direction was larger than that of the Ni(20$\bar{2}$) peak. These results strongly suggest that the h-BN(11$\bar{2}$0) planes were compressed due to the strain from the Ni(111) surface to form a heteroepitaxial relationship of h-BN(11$\bar{2}$0)||Ni(20$\bar{2}$) (or h-BN(10$\bar{1}$0)||Ni(11$\bar{2}$)).[23,24]

Microstructural analysis

The crystal structure and crystallinity of the h-BN film were studied further using SAED. Figure 5a illustrates our SAED measurements at different positions distributed over a large area.[39] As shown in the left image in Figure 5b, first, the SAED measured with a 4.5-μm aperture clearly showed a single-oriented hexagonal crystal structure. Then, 16 SAED patterns were obtained in the same manner at different positions over a 0.3×0.3 mm^2 area. The obtained images were overlapped into a single image (middle in Figure 5b). Because all the patterns were almost identical, the overlapped image was similar to each individual pattern. This indicates that the SAED patterns originated from a single h-BN domain over the 0.3×0.3 mm^2 region. To investigate the crystallinity over an even larger area, nine SAED patterns were obtained at the center and corners of a 0.9×0.9 mm^2 area using a 20-μm aperture. The obtained pattern images were overlapped again into a single image (right in Figure 5b). Similarly, no significantly different crystal orientations were observed, which indicates that the SAED patterns still belonged to the same single h-BN domain over the 0.9×0.9 mm^2 area. Meanwhile, as the measurement area became wider, the dispersion of the (10$\bar{1}$0) spot increased from 2.9° to 4.4° and then to 7.1° (left, middle and right in Figure 5b, respectively). This broadening may be attributed to the accidental folding of h-BN layers introduced during the wet transfer process.

Electron back-scattered diffraction accompanied by TEM (TEM-EBSD) enables the spatial mapping of the crystal orientation of h-BN in the nanometer scale.[40] In TEM-EBSD, a nanometer-sized electron beam probe performs point-by-point scans of the specimen, after which the crystal orientation mapping image is constructed using the electron diffraction pattern at each point (Figure 5c). Figure 5d shows the inverse pole figure (IPF) map with color legends over a 3×3 μm^2 area of a h-BN film in the normal direction (ND) and transverse direction (TD). The colors represent the crystallographic orientation with respect to each direction of the sample. In the left image in Figure 5d, the entire region of the image is colored in red, which corresponds to the (0001) plane of the hexagonal structure of h-BN aligned to ND in the whole region of the image. The black points in the image are caused by the low signal-to-noise ratio, limited by the small thickness of the sample and integration time during scanning, which hinders the determination of the crystallographic information within the desired accuracy requirements. The IPF map in TD presented in the right image in Figure 5d shows a similar result with the entire region of the image colored in green, which corresponded to the (2$\bar{1}\bar{1}$0) plane of the sample aligned to TD.

The atomic structure of h-BN films was also investigated using high-resolution TEM, which was obtained by Cs aberration-corrected low acceleration voltage TEM. Figure 5e shows an high-resolution

TEM image of an h-BN film, where the hexagonal structure of h-BN layers can be clearly observed. The *d*-spacing value of the $(10\bar{1}0)$ lattice planes obtained from the image, $d = 2.18$ Å, agrees well with the known *d*-spacing value of h-BN $(10\bar{1}0)$ lattice planes, $d = 2.17$ Å.[41] The fast-Fourier-transformed image in the inset of Figure 5e also confirms that the hexagonal lattice is single-orientated. Nanometer- and atomic-resolution imaging using TEM-EBSD and high-resolution TEM strongly suggest that the h-BN films are single-oriented and free of nanometer-sized grain boundaries or turbostratic crystalline structures.

CONCLUSION

In conclusion, centimeter-scale epitaxial h-BN layers were successfully grown and separated from Ni(111) single crystal substrates by combining chemical vapor deposition growth of h-BN with the bubbling transfer technique. The optimal source sublimation and growth temperatures were found to be important for synthesizing few-layered h-BN with full coverage and high crystallinity, while the cooling rate had a negligible role. Over-repeated growth and transfer processes after the initial annealing, no significant degradation of Ni(111) substrates was observed, and the crystallinity of h-BN layers was reproduced reliably. Using high-resolution SR-XRD, the h-BN films were confirmed to be single domain over a centimeter-scale area, and h-BN and Ni were found to form a heteroepitaxial relationship of h-BN(0002) ‖ Ni(111) and h-BN$(11\bar{2}0)$ ‖ Ni$(20\bar{2})$ (or h-BN$(10\bar{1}0)$ ‖ Ni$(11\bar{2})$). The microstructural analysis using TEM indicated that the grown h-BN layers were of high crystallinity, and the layers have uniform crystallographic orientation over the entire region. In particular, structural distortions or nanometer-sized defects were not observed even at nanometer and atomic scales. The grown h-BN films showed typical physical characteristics of h-BN, with a high uniformity over a wide area. The large-area synthesis and transfer of atomically thin uniform epitaxial h-BN layers can be applied in various fields where high-quality two-dimensional insulating layers are required.

CONFLICT OF INTEREST

The authors declare no conflict of interest.

ACKNOWLEDGEMENTS

This work was financially supported by the Samsung Research Funding Center of Samsung Electronics (SRFC-TA1503-05). The work by JJ and MK was supported by the NRF grant funded by the MSIP (NO NRF-2015055406). SEM-EBSD, TEM and TEM-EBSD analyses were supported by the Research Institute of Advanced Materials (RIAM) in Seoul National University, Seoul, Korea. Cs-corrected high-resolution TEM image analysis was supported by the Korea Institute of Science and Technology (KIST) in Jeonbuk, Korea.

1 Watanabe, K., Taniguchi, T. & Kanda, H. Direct-bandgap properties and evidence for ultraviolet lasing of hexagonal boron nitride single crystal. *Nat. Mater.* **3**, 404–409 (2004).
2 Jo, I., Pettes, M. T., Kim, J., Watanabe, K., Taniguchi, T., Yao, Z. & Shi, L. Thermal conductivity and phonon transport in suspended few-layer hexagonal boron nitride. *Nano Lett.* **13**, 550–554 (2013).
3 Kim, K. K., Kim, S. M. & Lee, Y. H. A new horizon for hexagonal boron nitride film. *J. Korean Phys. Soc.* **64**, 1605–1616 (2014).
4 Pakdel, A., Bando, Y. & Golberg, D. Nano boron nitride flatland. *Chem. Soc. Rev.* **43**, 934–959 (2014).
5 Chung, K., Lee, C. H. & Yi, G. C. Transferable GaN layers grown on ZnO-coated graphene layers for optoelectronic devices. *Science* **330**, 655–657 (2010).
6 Kobayashi, Y., Kumakura, K., Akasaka, T. & Makimoto, T. Layered boron nitride as a release layer for mechanical transfer of GaN-based devices. *Nature* **484**, 223–227 (2012).
7 Lee, G. H., Yu, Y. J., Cui, X., Petrone, N., Lee, C. H., Choi, M. S., Lee, D. Y., Lee, C., Yoo, W. J., Watanabe, K., Taniguchi, T., Nuckolls, C., Kim, P. & Hone, J. Flexible and transparent MoS2 field-effect transistors on hexagonal boron nitride-graphene heterostructures. *ACS Nano* **7**, 7931–7936 (2013).
8 Oh, H., Hong, Y. J., Kim, K.-S., Yoon, S., Baek, H., Kang, S.-H., Kwon, Y.-K., Kim, M. & Yi, G.-C. Architectured van der Waals epitaxy of ZnO nanostructures on hexagonal BN. *NPG Asia Mater.* **6**, e145 (2014).
9 Petrone, N., Cheri, T., Meric, I., Wang, L., Shepard, K. L. & Hone, J. Flexible graphene field-effect transistors encapsulated in hexagonal boron nitride. *ACS Nano* **9**, 8953–8959 (2015).
10 Dean, C. R., Young, A. F., Meric, I., Lee, C., Wang, L., Sorgenfrei, S., Watanabe, K., Taniguchi, T., Kim, P., Shepard, K. L. & Hone, J. Boron nitride substrates for high-quality graphene electronics. *Nat. Nanotechnol.* **5**, 722–726 (2010).
11 Xue, J., Sanchez-Yamagishi, J., Bulmash, D., Jacquod, P., Deshpande, A., Watanabe, K., Taniguchi, T., Jarillo-Herrero, P. & LeRoy, B. J. Scanning tunnelling microscopy and spectroscopy of ultra-flat graphene on hexagonal boron nitride. *Nat. Mater.* **10**, 282–285 (2011).
12 Shi, Y. M., Hamsen, C., Jia, X. T., Kim, K. K., Reina, A., Hofmann, M., Hsu, A. L., Zhang, K., Li, H. N., Juang, Z. Y., Dresselhaus, M. S., Li, L. J. & Kong, J. Synthesis of few-layer hexagonal boron nitride thin film by chemical vapor deposition. *Nano Lett.* **10**, 4134–4139 (2010).
13 Song, L., Ci, L. J., Lu, H., Sorokin, P. B., Jin, C. H., Ni, J., Kvashnin, A. G., Kvashnin, D. G., Lou, J., Yakobson, B. I. & Ajayan, P. M. Large scale growth and characterization of atomic hexagonal boron nitride layers. *Nano Lett.* **10**, 3209–3215 (2010).
14 Kim, G., Jang, A. R., Jeong, H. Y., Lee, Z., Kang, D. J. & Shin, H. S. Growth of high-crystalline, single-layer hexagonal boron nitride on recyclable platinum foil. *Nano Lett.* **13**, 1834–1839 (2013).
15 Tay, R. Y., Griep, M. H., Mallick, G., Tsang, S. H., Singh, R. S., Tumlin, T., Teo, E. H. T. & Karna, S. P. Growth of large single-crystalline two-dimensional boron nitride hexagons on electropolished copper. *Nano Lett.* **14**, 839–846 (2014).
16 Wu, Q. K., Park, J. H., Park, S., Jung, S. J., Suh, H., Park, N., Wongwiriyapan, W., Lee, S., Lee, Y. H. & Song, Y. J. Single crystalline film of hexagonal boron nitride atomic monolayer by controlling nucleation seeds and domains. *Sci. Rep.* **5**, 16159 (2015).
17 Liu, Y. Y., Zou, X. L. & Yakobson, B. I. Dislocations and grain boundaries in two-dimensional boron nitride. *ACS Nano* **6**, 7053–7058 (2012).
18 Wang, Z. G. Structure and electronic properties of boron nitride sheet with grain boundaries. *J. Nanopart. Res.* **14**, 756 (2012).
19 Ding, N., Wu, C. M. L. & Li, H. The effect of grain boundaries on the mechanical properties and failure behavior of hexagonal boron nitride sheets. *Phys. Chem. Chem. Phys.* **16**, 23716–23722 (2014).
20 Li, Q. C., Zou, X. L., Liu, M. X., Sun, J. Y., Gao, Y. B., Qi, Y., Zhou, X. B., Yakobson, B. I., Zhang, Y. F. & Liu, Z. F. Grain boundary structures and electronic properties of hexagonal boron nitride on Cu(111). *Nano Lett.* **15**, 5804–5810 (2015).
21 Brown, L., Lochocki, E. B., Avila, J., Kim, C. J., Ogawa, Y., Havener, R. W., Kim, D. K., Monkman, E. J., Shai, D. E., Wei, H. F. I., Levendorf, M. P., Asensio, M., Shen, K. M. & Park, J. Polycrystalline graphene with single crystalline electronic structure. *Nano Lett.* **14**, 5706–5711 (2014).
22 Lu, G., Wu, T., Yuan, Q., Wang, H., Wang, H., Ding, F., Xie, X. & Jiang, M. Synthesis of large single-crystal hexagonal boron nitride grains on Cu-Ni alloy. *Nat. Commun.* **6**, 6160 (2015).
23 Auwarter, W., Kreutz, T. J., Greber, T. & Osterwalder, J. XPD and STM investigation of hexagonal boron nitride on Ni(111). *Surf. Sci.* **429**, 229–236 (1999).
24 Oshima, C., Itoh, A., Rokuta, E., Tanaka, T., Yamashita, K. & Sakurai, T. A hetero-epitaxial-double-atomic-layer system of monolayer graphene/monolayer h-BN on Ni(111). *Solid State Commun.* **116**, 37–40 (2000).
25 Auwarter, W., Muntwiler, M., Osterwalder, J. & Greber, T. Defect lines and two-domain structure of hexagonal boron nitride films on Ni(111). *Surf. Sci.* **545**, L735–L740 (2003).
26 Greber, T. in *Handbook of Nanophysics. Functional Nanomaterials* (ed. Sattler K. D.) 18-1–18-22 (Taylor & Francis: Boca Raton, 2011).
27 Auwarter, W., Suter, H. U., Sachdev, H. & Greber, T. Synthesis of one monolayer of hexagonal boron nitride on Ni(111) from B-trichloroborazine (ClBNH)(3). *Chem. Mater.* **16**, 343–345 (2004).
28 Greber, T., Brandenberger, L., Corso, M., Tamai, A. & Osterwalder, J. Single layer hexagonal boron nitride films on Ni(110). *e-J. Surf. Sci. Nanotechnol.* **4**, 410–413 (2006).
29 Goriachko, A. & Over, H. Modern nanotemplates based on graphene and single layer h-BN. *Z Phys. Chem.* **223**, 157–168 (2009).
30 Yuzuriha, T. H. & Hess, D. W. Structural and optical-properties of plasma-deposited boron-nitride films. *Thin Solid Films* **140**, 199–207 (1986).
31 Wang, Y., Zheng, Y., Xu, X. F., Dubuisson, E., Bao, Q. L., Lu, J. & Loh, K. P. Electrochemical delamination of CVD-grown graphene film: toward the recyclable use of copper catalyst. *ACS Nano* **5**, 9927–9933 (2011).
32 Kim, K. K., Hsu, A., Jia, X. T., Kim, S. M., Shi, Y. M., Dresselhaus, M., Palacios, T. & Kong, J. Synthesis and characterization of hexagonal boron nitride film as a dielectric layer for graphene devices. *ACS Nano* **6**, 8583–8590 (2012).
33 Lee, Y. H., Liu, K. K., Lu, A. Y., Wu, C. Y., Lin, C. T., Zhang, W. J., Su, C. Y., Hsu, C. L., Lin, T. W., Wei, K. H., Shi, Y. M. & Li, L. J. Growth selectivity of hexagonal-boron nitride layers on Ni with various crystal orientations. *RSC Adv.* **2**, 111–115 (2012).
34 Cho, H., Park, S., Won, D. I., Kang, S. O., Pyo, S. S., Kim, D. I., Kim, S. M., Kim, H. C. & Kim, M. J. Growth kinetics of white graphene (h-BN) on a planarised Ni foil surface. *Sci. Rep.* **5**, 11985 (2015).

35 Park, J. H., Park, J. C., Yun, S. J., Kim, H., Luong, D. H., Kim, S. M., Choi, S. H., Yang, W., Kong, J., Kim, K. K. & Lee, Y. H. Large-area monolayer hexagonal boron nitride on Pt foil. *ACS Nano* **8**, 8520–8528 (2014).
36 Kim, S. M., Hsu, A., Park, M. H., Chae, S. H., Yun, S. J., Lee, J. S., Cho, D. H., Fang, W., Lee, C., Palacios, T., Dresselhaus, M., Kim, K. K., Lee, Y. H. & Kong, J. Synthesis of large-area multilayer hexagonal boron nitride for high material performance. *Nat. Commun.* **6**, 8662 (2015).
37 JCPDS–International Centre for Diffraction Data & International Centre for Diffraction Data. *Powder Diffraction File* (International Centre for Diffraction Data: Newtown Square, PA, USA, 1993).
38 Wang, W. L., Yang, W. J., Liu, Z. L., Lin, Y. H., Zhou, S. Z., Qian, H. R., Wang, H. Y., Lin, Z. T., Zhang, S. G. & Li, G. Q. Synthesis of homogeneous and high-quality GaN films on Cu(111) substrates by pulsed laser deposition. *CrystEngComm.* **16**, 8500–8507 (2014).
39 Yan, Z., Lin, J., Peng, Z. W., Sun, Z. Z., Zhu, Y., Li, L., Xiang, C. S., Samuel, E. L., Kittrell, C. & Tour, J. M. Toward the synthesis of wafer-scale single-crystal graphene on copper foils. *ACS Nano* **6**, 9110–9117 (2012).
40 Galand, R., Brunetti, G., Arnaud, L., Rouviere, J. L., Clement, L., Waltz, P. & Wouters, Y. Microstructural void environment characterization by electron imaging in 45 nm technology node to link electromigration and copper microstructure. *Microelectron. Eng.* **106**, 168–171 (2013).
41 Xue, Y. F., Liu, Q., He, G. J., Xu, K. B., Jiang, L., Hu, X. H. & Hu, J. Q. Excellent electrical conductivity of the exfoliated and fluorinated hexagonal boron nitride nanosheets. *Nanoscale Res. Lett.* **8**, 49 (2013).

Supplementary Information accompanies the paper on the NPG Asia Materials website (http://www.nature.com/am)